Supplementary Information

Amorphous iron vanadate positive electrode enabling fast pseudocapacitive sodium-ion storage

Xiaoqing Chang†, Dafu Tang†, Sicheng Fan, Guiyang Gao, Qiulong Wei*

State Key Laboratory of Physical Chemistry of Solid Surfaces, Fujian Key Laboratory of Surface and Interface Engineering for High Performance Materials, College of Materials, Xiamen University, Xiamen 361005, China

*E-mail: qlwei@xmu.edu.cn

Experimental Section

Materials synthesis

Amorphous iron vanadate (*a*-FVO) was synthesized using the previously reported method.[1] 2 mmol of iron (II) acetylacetonate and 2, 4 or 8 mmol of vanadyl acetylacetonate were added into 70 mL ethylene glycol solution. The mixture was stirred for 24 h to form a uniform solution at room temperature, and then transferred into a 100 mL Teflon-lined stainless-steel autoclave and held at 150 °C for 24 h. After the solution cooled to room temperature, the precipitate was collected by centrifugation and washed alternately with deionized water and ethanol for three times. The *a*-FVO powder was obtained after being dried at 80 °C under vacuum overnight followed by annealing treatment at 250 °C for 2 h in air to remove impurities. The crystalline F1V2O was obtained through annealing treatment at 500 °C for 2 h in air.

Material characterization

Inductively coupled plasma optical emission spectroscopy (ICP-OES) measurements were conducted on Thermo SCIENTIFIC iCAP7400. Powder X-ray diffraction (XRD) patterns were recorded on a Bruker D8 Advance X-ray diffractometer (Cu Kα radiation, λ=1.54056 Å). Raman spectroscopy were performed using a laser wavelength of 532 nm to acquire data in the high-resolution Raman spectrometer (HORIBA HR Evolution). Brunauer–Emmett–Teller (BET) specific surface area was measured via nitrogen sorption isotherms (Micromeritics Tristar 3020) at 77 K after degassing under vacuum at 120 °C for 6 h. Scanning electron microscopy (SEM) images and Energy Dispersive Spectroscopy (EDS) elemental mappings were collected on a Zeiss Sigma 300. For ex situ XRD and Raman spectroscopy characterizations, the coin cells that reached the required states were disassembled in an Ar-filled glove box, and the electrodes were washed with diglyme and then tested.

Electrode preparation

The *a*-FVO electrodes were prepared by mixing 85 wt.% the as-synthesized *a*-FVO powder, 10 wt.% Ketjet black (EC-600JD, Nouryon), and 5 wt.% polyvinylidene fluoride (PVDF, Arkema) in N-methylpyrrolidone (NMP, >99%, Acmec) solution to form a slurry and then

coated onto an Al foil using doctor blading. The mass loading of active materials is controlled at ~2.5 mg cm^{-2}. The electrodes were dried at 120 °C for 12 h under vacuum and cut into 12 mm diameter discs using a punching machine.

Electrochemical measurements

Coin cells (CR2032) were assembled in an Ar-filled glove box with O_2 < 0.1 ppm and H_2O < 0.1 ppm. A sodium metal disk was used as the counter and reference electrode. A Celgard-2325 membrane was used as separator. 1 M $NaPF_6$ in diglyme (80 μL, >99.7%, DuoDuo Chemical Technology Co.) used as electrolyte. The cyclic voltammetry (CV) and galvanostatic charge and discharge measurements were measured by the electrochemical workstation (Bio-Logic VSP) and NEWARE battery test system (CT-9008), respectively. Electrochemical impedance spectroscopy (EIS) measurements were conducted on the Bio-Logic VSP potentiostat by a potentiostatic method with an applied amplitude of 10 mV in the range of 200 kHz to 10 mHz. The galvanostatic intermittent titration technique (GITT) was performed with a constant current discharge at 0.02 A g^{-1} for 10 min followed by relaxation for 1.5 h on the NEWARE Battery Test System.

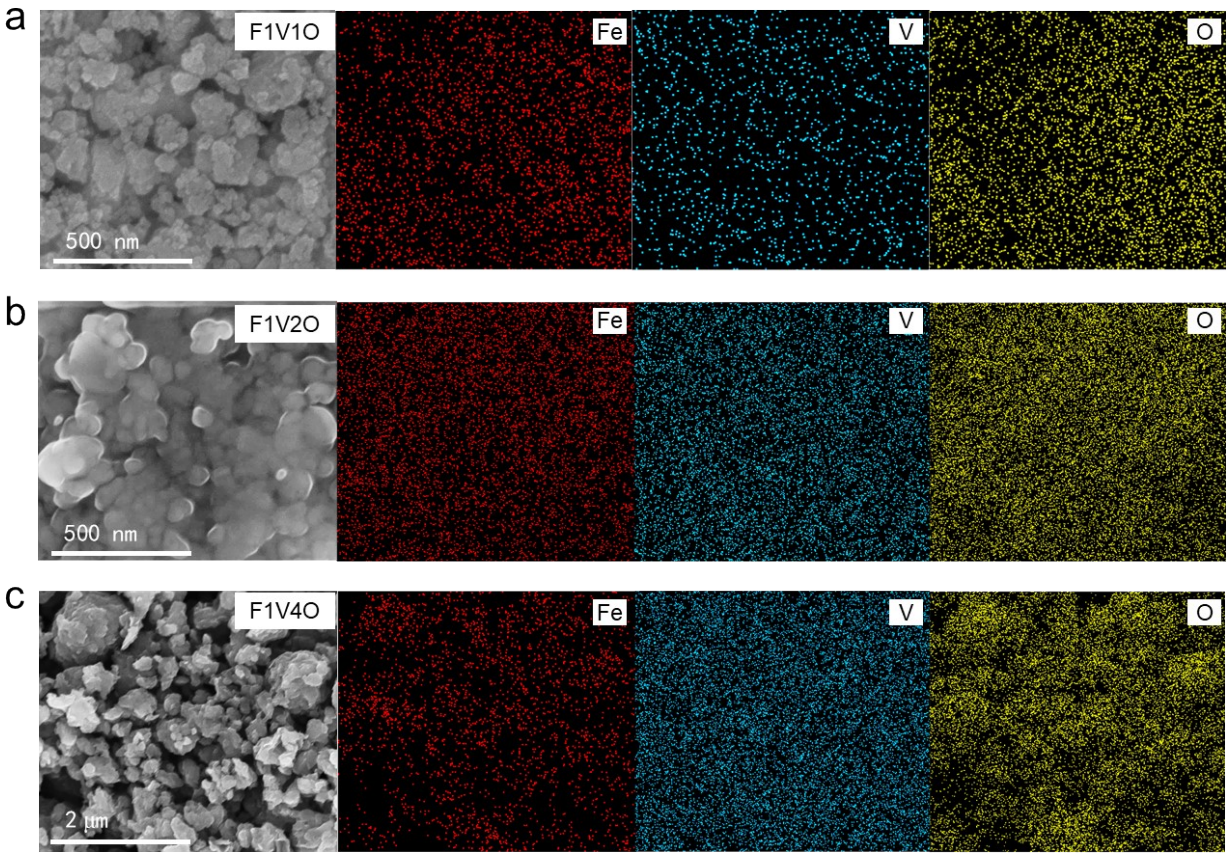

Fig. S1 SEM images and element mappings of (a) F1V1O, (b) F1V2O and (c) F1V4O samples.

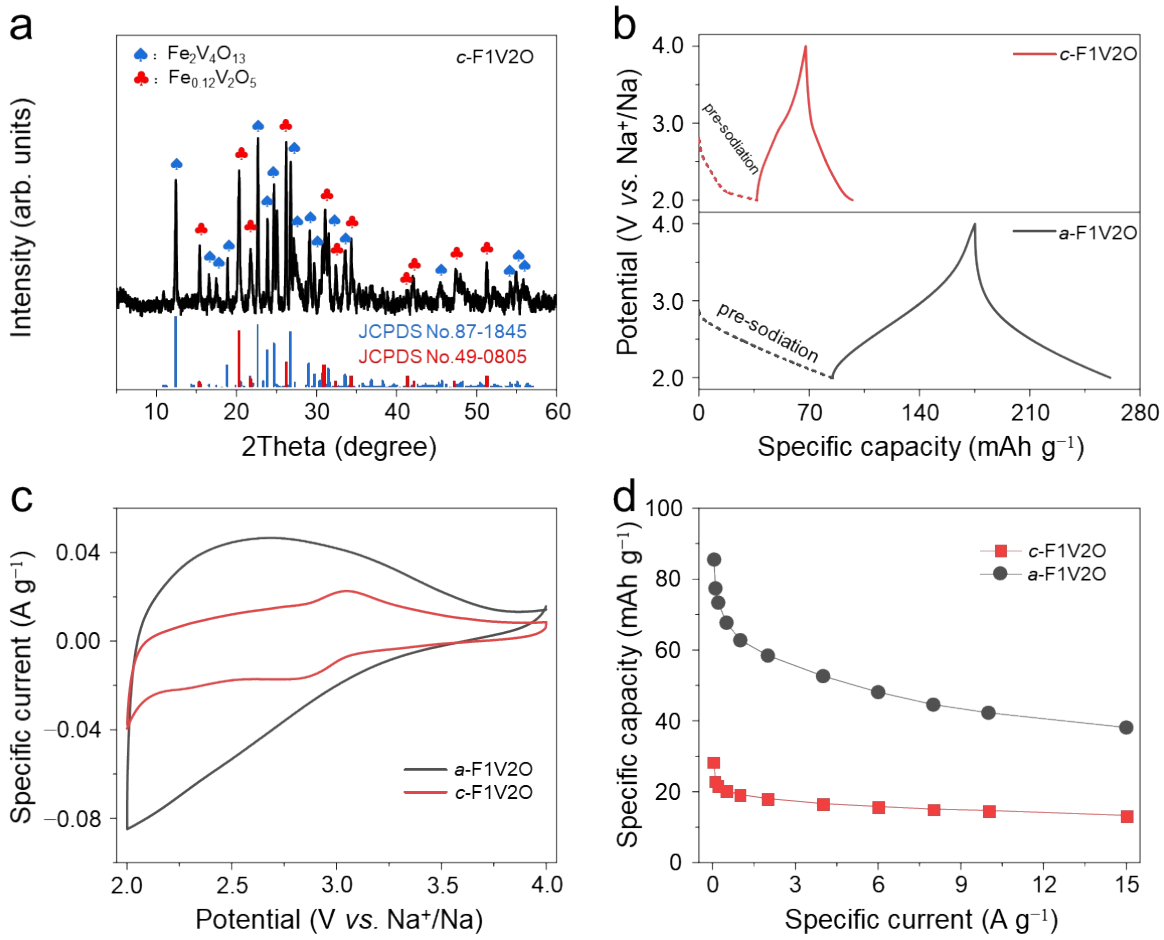

Fig. S2 (a) XRD pattern of the synthesized *c*-F1V2O sample, (b) GCD curves for initial 2 cycles, (c) CV curves for the 5th cycle and (d) rate performance of *a*-F1V2O and *c*-F1V2O positive electrodes.

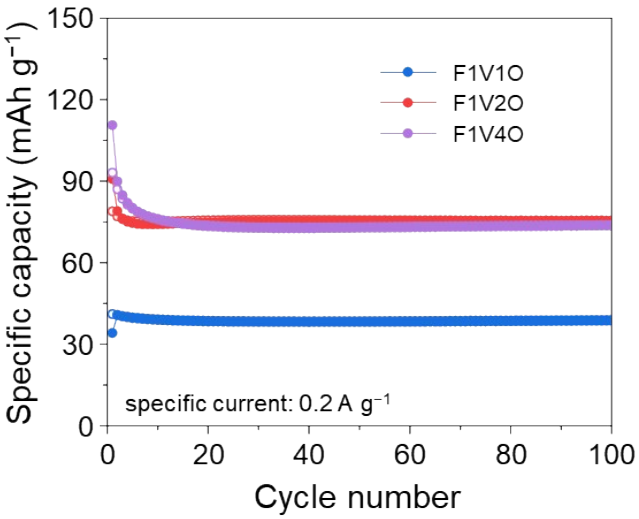

Fig. S3 Cycling performance of the three *a*-FVO positive electrodes at 0.2 A g^{-1}.

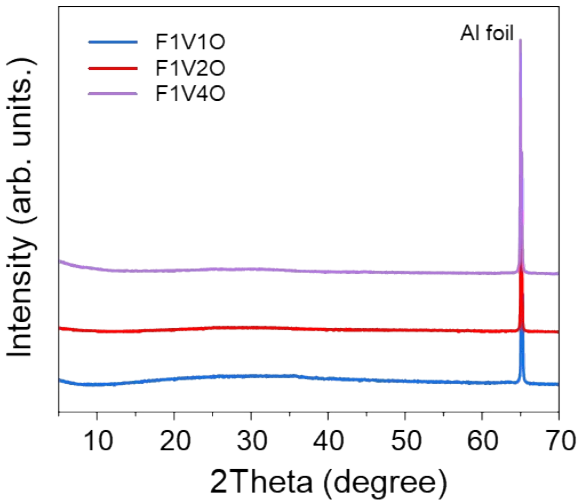

Fig. S4 XRD patterns of three *a*-FVO positive electrodes after 1000 cycles at 1 A g^{-1}.

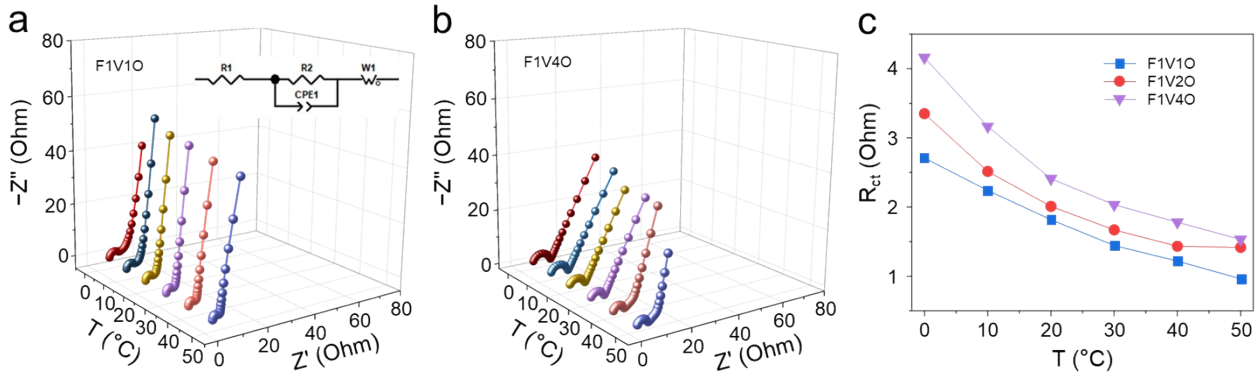

Fig. S5 Nyquist plots of the (a) F1V1O and (b) F1V4O electrodes at various temperatures (Insert is the equivalent circuit model). (c) Fitted R_{ct} value of the three *a*-FVO electrodes at various temperatures.

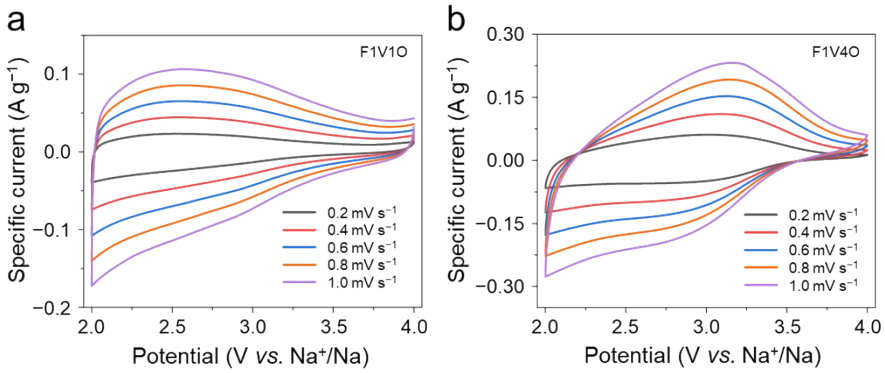

Fig. S6 CV curves of the (a) F1V1O and (b) F1V4O electrodes at various sweep rates.

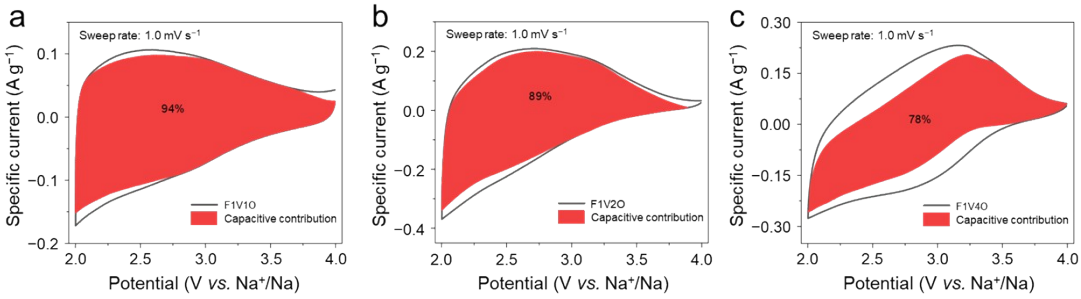

Fig. S7 Capacitive contributions to sodium-ion storage for the (a) F1V1O, (b) F1V2O and (c) F1V4O electrodes at 1 mV s^{-1}.

Table S1 The initial Coulombic efficiency of the three *a*-FVO positive electrodes.

Positive electrode	Initial desodiation capacity at 0.05 A g^{-1} (mAh g^{-1})	Initial sodiation capacity at 0.05 A g^{-1} (mAh g^{-1})	Initial Coulombic efficiency (%)
F1V1O	38.6	42.4	109.9
F1V2O	90.4	85.9	95.0
F1V4O	108.4	101.1	93.3

Table S2. The electrochemical properties of pseudocapacitive positive electrodes reported previously.

Positive electrodes	Mass loading (mg cm^{-2})	Potential window (V)	Specific capacity (xx mAh g^{-1} at xx A g^{-1})	Rate performance (xx mAh g^{-1} at xx A g^{-1})	Cycle life	Ref.
F1V2O	1.5−2	2−4	85 at 0.05	38.2 at 15	105% after 1000 cycles at 1 A g^{-1}	This work
$VOPO_4$ NS	1	2.5−4.3	114 at 0.08	48 at 1.67	73% after 500 cycles at 0.83 A g^{-1}	2
PB-A	–	2−4	92 at 0.5 C	55 at 3	70% after 1000 cycles at 1 C.	3
LV-CuHCF	1−2	2−4	86 at 0.08	41 at 8	56% after 1000 cycles at 0.8 A g^{-1}	4
K-MDC(0)	2−4	2.0−4.2	70 at 0.1	40 at 10	82% after 5000 cycles at 2 A g^{-1}	5
IE-NMO10	1−2	2−4	94 at 0.06	45 at 2.4	98.1% after 1000 cycles at 2.4 A g^{-1}	6
SOPC-10	2	1.2−4.2	87 at 0.05	50 at 10	25% after 2500 cycles at 1 A g^{-1}	7
NVO-0.01Nb	–	1.5−4.0	85 at 0.03	30 at 0.24	40% after 500 cycles at 0.12 A g^{-1}	8
NMZP@C-rGO	1.6−1.8	2.5−4.3	100 at 0.05	50.9 at 5	97.4% after 1500 cycles at 0.02 A g^{-1}	9

Reference

1 Y. Jiang, F. Wu, Z. Ye, C. Li, Y. Zhang, L. Li, M. Xie and R. Chen, *Adv. Funct. Mater.*, 2021, **31**, 2009756.

2 Y. Zhu, L. Peng, D. Chen and G. Yu, *Nano Lett.*, 2016, **16**, 742−747.

3 Y. Chen, H. J. Woo, S. A. F. Syed Mohd Fadzil, W. Tan, F. Wang and A. K. Mohd Arof, *ACS Appl. Nano Mater.*, 2022, **5**, 4833−4840.

4 B. Wang, S. Liu, W. Sun, Y. Tang, H. Pan, M. Yan and Y. Jiang, *ChemSusChem*, 2019, **12**, 2415−2420.

5 Y. M. Jung, J. H. Choi, D. W. Kim and J. K. Kang, *Adv. Sci.*, 2023, **10**, 2301160.

6 Y. Cao, M. Xiao, W. Dong, T. Cai, H. Bi and F. Huang, *Sci. China Mater.*, 2023, **66**, 3810−3816.

7 W. Ren, Y. Xiong, L. Yang, Y. Zhang, H. Liang, C. Zhu, X. Wang, J. Chen, W. Tian and M. Huang, *Carbon*, 2025, **238**, 120245.

8 L. Zhu, C. Pan, Q. Han, Y. Miao, X. Yang, L. Xie and X. Cao, *J. Alloys Compd.*, 2022, **890**, 161885.

9 X. Ma, X. Wu, Y. Liu, W. Wu, Z. Pan and P. K. Shen, *ACS Appl. Mater. Interfaces*, 2021, **13**, 21390−21400.